

## A sustainable strategy for Open Streets in (post) pandemic cities

Daniel Rhoads<sup>1</sup>, Albert Solé-Ribalta<sup>1,2</sup>, Marta C. González <sup>3,4,5</sup> & Javier Borge-Holthoefer <sup>1</sup>✉

Cities world-wide have taken the opportunity presented by the COVID-19 pandemic to improve and expand pedestrian infrastructure, providing residents with a sense of relief and pursuing long-standing goals to decrease automobile dependence and increase walkability. So far, due to a scarcity of data and methodological shortcomings, these efforts have lacked the system-level view of treating sidewalks as a network. Here, we leverage sidewalk data from ten cities in three continents, to first analyse the distribution of sidewalk and roadbed geometries, and find that cities present an unbalanced distribution of public space, favouring automobiles at the expense of pedestrians. Next, we connect these geometries to build a sidewalk network -adjacent, but irreducible to the road network. Finally, we compare a no-intervention scenario with a shared-effort heuristic, in relation to the performance of sidewalk infrastructures to guarantee physical distancing. The heuristic prevents the sidewalk connectivity breakdown, while preserving the road network's functionality.

<sup>1</sup>Internet Interdisciplinary Institute (IN3), Universitat Oberta de Catalunya, Barcelona, Catalonia, Spain. <sup>2</sup>URPP Social Networks, University of Zurich, Zurich, Switzerland. <sup>3</sup>Department of City and Regional Planning, University of California, Berkeley, CA, USA. <sup>4</sup>Energy Technologies Area, Lawrence Berkeley National Laboratory, Berkeley, CA, USA. <sup>5</sup>Department of Civil and Environmental Engineering, University of California, Berkeley, CA, USA.  
✉email: [jborgeh@uoc.edu](mailto:jborgeh@uoc.edu)

Called variously “Open”, “Slow”, “Safe”, or “Shared” streets, the vision of limiting traffic on urban roadways to free up public space for pedestrians and cyclists clearly predates 2019—but the pandemic crisis has emboldened it decisively. By 2021, it has become clear that outdoor transmission of SARS-CoV-2 is rare<sup>1</sup>, and yet a preceding lack of evidence, along with an exacerbated public risk perception based on uncertainty<sup>2–4</sup>, resulted in outdoor physical distancing recommendations, which in turn placed more pressure on streets in general, and sidewalks in particular. City-dwellers had then to learn on-the-fly how to move around in the public space of the city, while at the same time keeping a distance of at least 1.5 m from their fellow citizens<sup>5–7</sup>. It was at this point that cities world-wide took the opportunity presented by the pandemic to improve and expand pedestrian infrastructure<sup>8</sup>, not only to help people comply with recommendations, but also to promote social benefits in terms of health, environmental sustainability, and economics that are associated with active forms of transportation<sup>9,10</sup>.

Now, as vaccine-driven herd immunity presses ahead<sup>11</sup> in some countries, the long-term effects of the COVID-19 crisis on people’s daily habits remains unclear. Many public transit systems have not recovered from the precipitous drop in ridership seen over the past year<sup>12–14</sup>, while car use has remained steady, or is even expanding<sup>13</sup>. Furthermore, the potential emergence of new strains and future epidemics (for which outdoor transmissibility is unpredictable)<sup>15,16</sup> calls for better preparedness and planning. In this context, some cities are making Open Street programs permanent, but many others are not. Among those pushing for permanence, e.g., the C40 Cities Climate Leadership Group, there are common goals (sustainability, equitable space share, active mobility) but no clear city-level methodological guidelines. Should cities strive for distance goals (1, or 10, or 100 walkable kilometers)? Should they rather pay attention to routing and connectivity? Such a challenging shift in urban design calls for interdisciplinary efforts to understand how cities might be reformed efficiently and safely<sup>17</sup>, towards a more sustainable future.

While the term “public space” may conjure up images of parks and greenways<sup>18</sup>, we focus here on perhaps the most important—and surely the most overlooked—public space of all: the sidewalk. It is precisely on sidewalks that most cities have implemented ad hoc interventions (from temporary sidewalk widenings to complete pedestrianisation) to give pedestrians more space and to avoid large gatherings, measures which serve to provide people with a sense of relief—with evolutionary grounds<sup>19</sup>—in terms of perceived risk<sup>3,20,21</sup>. So far, these interventions have been mostly local and manual, and have not directly benefited from a complex systems approach of treating urban sidewalks as a network, in part due to a generalized lack of publicly available data on sidewalk infrastructure worldwide.

In this work, we address the problems of space equity and traffic-restricted streets from the perspective of complex networks. We bridge the mentioned data gap by collecting comprehensive datasets of sidewalk and road infrastructure from ten world cities across three continents. First, we quantify the share of public space allotted to pedestrians versus cars, taking the measure of “arrogance of space” as defined by Colville-Andersen<sup>22</sup> to a city-wide level, and showing for the first time, to the best of our knowledge, on such a large scale how planning choices can leave pedestrians with less room to walk. In addition to quantifying the need for space for pedestrians, it is also important to measure the overall connectivity of the sidewalk infrastructure. Thus, building from the same sidewalk geometry data, we develop a method to automatically construct city-scale sidewalk networks, which we apply to our cities of study. Next, we assess the potential decline in connectivity suffered by the sidewalk networks as a

consequence of social distancing recommendations, leveraging tools from percolation theory. Up to now, nearly no quantitative analysis exists, to the best of our knowledge, regarding the robustness of sidewalk networks, with or without social distancing considerations. Anchoring our analysis to the World Health Organization (WHO) and National Association of City Transportation Officials (NACTO) recommendations<sup>6,23</sup>, we provide a baseline from which to adjust urban infrastructure, considering the delicate trade-offs between the sidewalk and road networks. Our proposal can either be applied in the context of a pandemic—as an extraordinary and temporary intervention—, or as a long term strategy to rebalance the distribution of public space.

## Results

**From pedestrian space to sidewalk networks.** As a first step to quantify urban pedestrian space, we have collected geodatasets from ten cities distributed across three continents, each comprised of a set of road and sidewalk information representing the geographic extent of those two features (see Supplementary Note 1 for more information). From these data, we can map out the space allocated to cars and pedestrians respectively, both for the city as a whole and within specific districts (see Fig. 1). Even at a small scale (Fig. 1a), it is already apparent that area designated to vehicles takes most of street space in the scenes. Scaling up this analysis to the city-wide level (Fig. 1b), we see that, even in a best-case scenario (Paris, France), sidewalks occupy just under half of the available space ( $f_s = 0.44$ ); at the other extreme, Denver devotes as little as 16% of its public space to sidewalks. Moreover, these fractions are not homogeneously distributed across the urban landscape. Indeed, the arrogance of space<sup>22</sup> is, in general, aggravated as we move out from the city center, as can be seen in the case of Denver, where darker reds are concentrated in the peripheral areas surrounding the lighter downtown. However, exceptions do arise: in Paris, for example, districts with a higher share of sidewalk space are more evenly distributed throughout the city, possibly indicating enclaves of older, more walkable neighborhoods amid modernized, car-friendly areas.

Moving from a city-wide to a global scale, the box plots in (Fig. 1c) summarize the district-level street space distributions across all 10 cities of study. In the lower end of the distributions, a few cities present an alarming lack of sidewalk infrastructure, with some districts allocating just 10% of their street space to sidewalks. With the exceptions of Boston and Paris, which both present relatively compact distributions of sidewalk share, most of the cities exhibit large heterogeneities in their distributions of the space devoted to pedestrians. Note that the box plots in Fig. 1c have been organized in ascending order, taking the average fraction of sidewalk in each city as a criterium. Remarkably, this results in a natural ordering of the cities by continent.

This initial analysis provides a glimpse of how street space is currently distributed in cities around the world, and allows us to hypothesize that social distancing measures could pose a variety of challenges, both within cities and among countries and continents. Validating this requires us to look beyond share of space dedicated to pedestrians at a specific location, to the service that sidewalks provide as urban transportation infrastructure. To this end, it is necessary to translate sidewalk geometries into a connected structure: a sidewalk network.

Building mainly from planimetric data, we follow a minimalistic (yet accurate) approach to sidewalk network construction. First, a node is placed whenever pedestrians have the choice either to change direction, or to change the surface on which they are walking. As such, edges are laid to link two nodes on the same surface (e.g., two corners of a block), or else to link the closest node across the street (e.g., a crosswalk). The resulting structure is

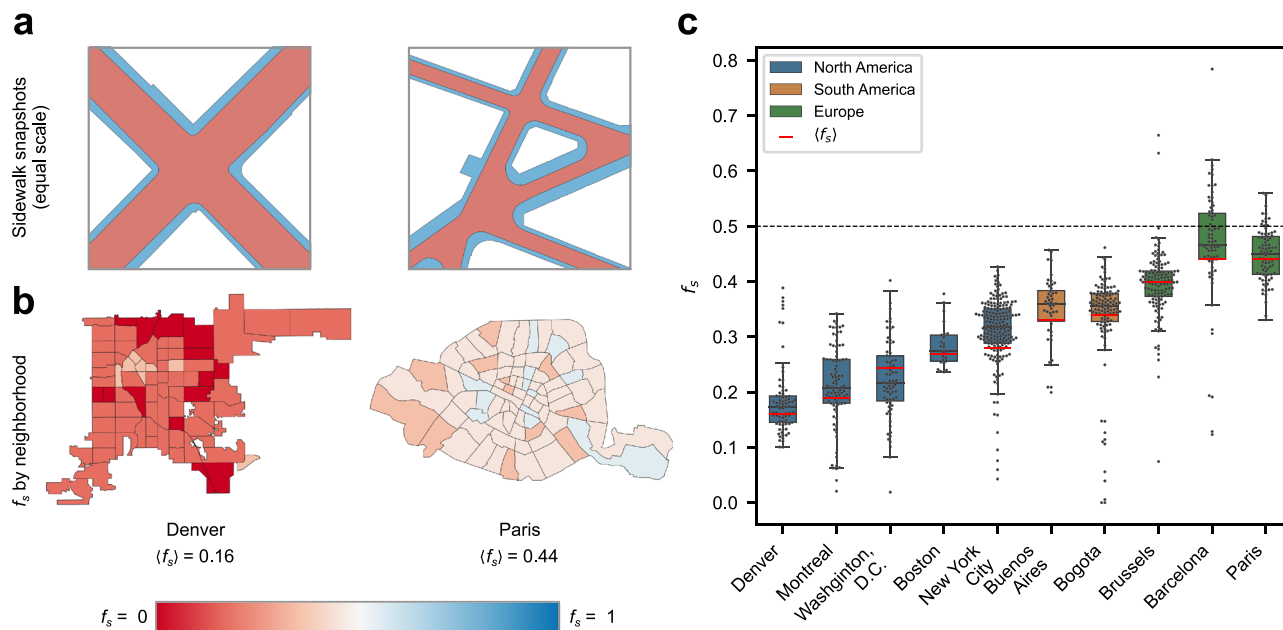


**Fig. 1 Maps and statistics on arrogance of space.** The distribution of street space between cars and pedestrians varies widely both within and among cities, but is everywhere biased towards cars. **a** Close-up snapshots representing the area for motor vehicles (red) and sidewalks (blue). White area corresponds to buildings. Clear to the naked eye, the majority of street space is devoted to cars. **b** A more general view of the cities under scrutiny confirms indeed that roads take up most of the space. Only Paris presents a few districts where the sidewalk share of street space  $f_s$  is above 50%. **c** Box plots (median in dark gray) displaying the distribution of space for all the cities for which the sidewalk geometries were gathered. The x-axis is sorted from lowest to highest average sidewalk share,  $\langle f_s \rangle$  marked in red. Interestingly, none of the cities achieve a median (nor average)  $f_s$  of 50% or higher. In general, cities present a remarkable internal heterogeneity, which implies that some districts (dots) suffer from a double inequity (with respect to cars, and also with respect to other areas of the city). It is clear that European cities rank best in the plot, possibly because they typically have larger “historical centers”, where street space tends to be shared.

an undirected, spatially-embedded, weighted network, where edges can be assigned a variety of relevant attributes (length, width, slope, etc.). A detailed description of the network construction process can be found in the Supplementary Note 1.

**Physical distancing on sidewalk networks.** With our newly-constructed sidewalk networks at hand, we can proceed to engage the problem of social distancing on sidewalks in a systematic way, as has been done with respect to other contexts such as public transportation<sup>24,25</sup>. In this section, we first test the networks’ present capability to provide for recommended safe distancing. We then go on to assess the potential of an automated heuristic to improve the current situation, emphasising sidewalk connectivity, as well as trade-offs with the urban road network.

*Status quo.* The natural approach to assessing the feasibility of interpersonal distancing on sidewalks from a network perspective is through targeted edge percolation. Percolation theory has been used to gain insights into a wide range of structural and behavioral features of networked systems, such as robustness, epidemic spreading, vital node identification, or community detection<sup>26</sup>, and has been extensively employed in the urban context<sup>27–30</sup>, also in relation to walkability<sup>31</sup>. Applied to our problem, targeted edge percolation translates to removing sidewalk segments that cannot guarantee a prescribed distance between people. Note that this does not translate to advocating the blockage of insufficiently-wide sidewalks as a policy. Instead, we take a similar perspective to Li et al.<sup>27</sup> by identifying certain network edges as dysfunctional. In our case, this occurs at the point in which the sidewalk is too crowded to afford a given interpersonal distance, and a risk-averse pedestrian, due to subjective fears that might be more or less justified, would not use the

edge in order to avoid exposing herself to close contact with others.

Given the uneven distribution of activities and population across the city, it is of course possible that, for example, a narrow sidewalk is sufficient on a small street with little foot traffic. Similarly, the widest sidewalk on a commercial artery may not withstand strict inter-personal distancing, due to high foot traffic demand. To take this into account, we define the condition for sidewalk edge removal considering a combination of structural and dynamical aspects of the network, i.e., taking into account sidewalk width and pedestrian flows, respectively. Building from static information on the width of each sidewalk segment  $w$ , obtained in the previous section, we calculate the effective width  $w^{\text{eff}}$  per segment, which encodes information from the estimated pedestrian flows. Accordingly,  $w^{\text{eff}}$  decreases when the level of flow from a given side of the segment results in the formation of multiple lines of pedestrians; and increases to infinity when flows are sufficiently low that an encounter between two pedestrians coming from opposite directions is not likely. Pedestrian-only or shared-space streets, as well as crosswalks, also have their  $w^{\text{eff}}$  set to infinity, and are thus not removed. Figure 2a–d highlights the steps involved, and a detailed description of both processes –the estimation of pedestrian flows and the subsequent calculation of effective sidewalk width– can be found in “Methods”. Sidewalk segments are thus removed from the network if their effective width falls below a predetermined threshold  $\tau$ , which indicates a prescribed interpersonal distance, see Fig. 2e–f. Coherently,  $\tau$  is initially set to 0 and incremented until no more network edges may be removed.

Percolation analysis typically takes the relative size of the giant connected component (GCC) as a proxy for network functionality, since a minimally functional network should provide for movement between a large enough fraction of nodes. While

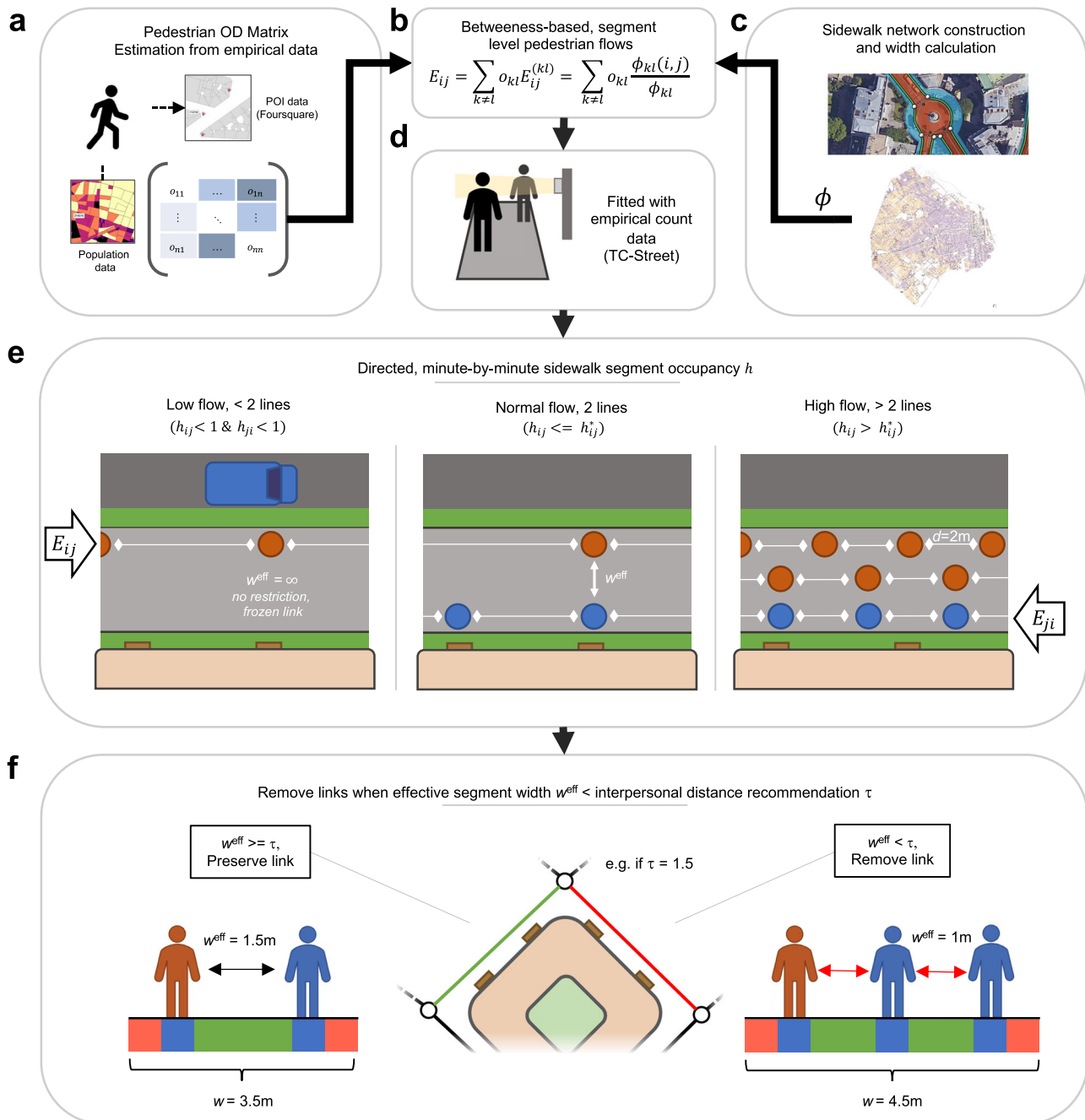


**Fig. 2 Sidewalk occupancy estimation.** **a–d** The effective width of a sidewalk ( $w^{\text{eff}}$ ) encapsulates a sidewalk’s structural (physical) aspects, and its dynamical performance in terms of pedestrian traffic. The dynamical aspects are estimated with a number of steps that include **(a)** demographic and service-location (POI: points-of-interest) aspects (pedestrian origin-destination matrix), **(b)** edge betweenness-based ( $E_{ij}$ ) pedestrian flow, and **(d)** empirical calibration from actual sidewalk occupancy data. The physical attributes **(c)** are those related with the sidewalk network construction and Geographic Information Systems (GIS) operations involved (see Supplementary Note 1), from which shortest path counts  $\phi$  can be obtained. **e** This pipeline results in the simplified consideration of a number of walking lines (pedestrians are represented as orange and blue dots), which determine, given the raw width of a sidewalk, how much space between lines is available ( $w^{\text{eff}}$ ). **f** In turn,  $w^{\text{eff}}$  is the attribute guiding the percolation protocol. In the example, the segment on the left allows 1.5 m between pedestrians, and is not removed (green); on the contrary, the segment on the right can only guarantee  $w^{\text{eff}} = 1\text{ m}$ , and for  $\tau = 1.5$  it will be removed (red color). Maps in **(a)** derived from municipal open data sources (see Supplementary Table 1). Imagery in **(c)** courtesy of: Google, © 2021 Aerodata International Surveys, CNES / Airbus, Maxar Technologies. Street networks in **(c)** courtesy of OpenStreetMap Contributors.

pedestrian behavior is known to be highly distance-constrained<sup>32</sup>, the GCC provides a clear indicator of system-level connectivity that is relevant regardless of the fact that agents on the network mostly perform their dynamics on a local scale<sup>31</sup>. Thus, as  $\tau$  increases, we monitor the relative size of the GCC, defined as a

fraction of the largest connected component,  $C_1$ , and the network size,  $N$ :  $\text{GCC} = C_1/N$ . The GCC informs us to what extent the network is still functional<sup>27,30</sup>, i.e., navigable. As a reference, we will focus on 1.5 and 2 m, which can be regarded as the minimal width range necessary for an individual to maintain social

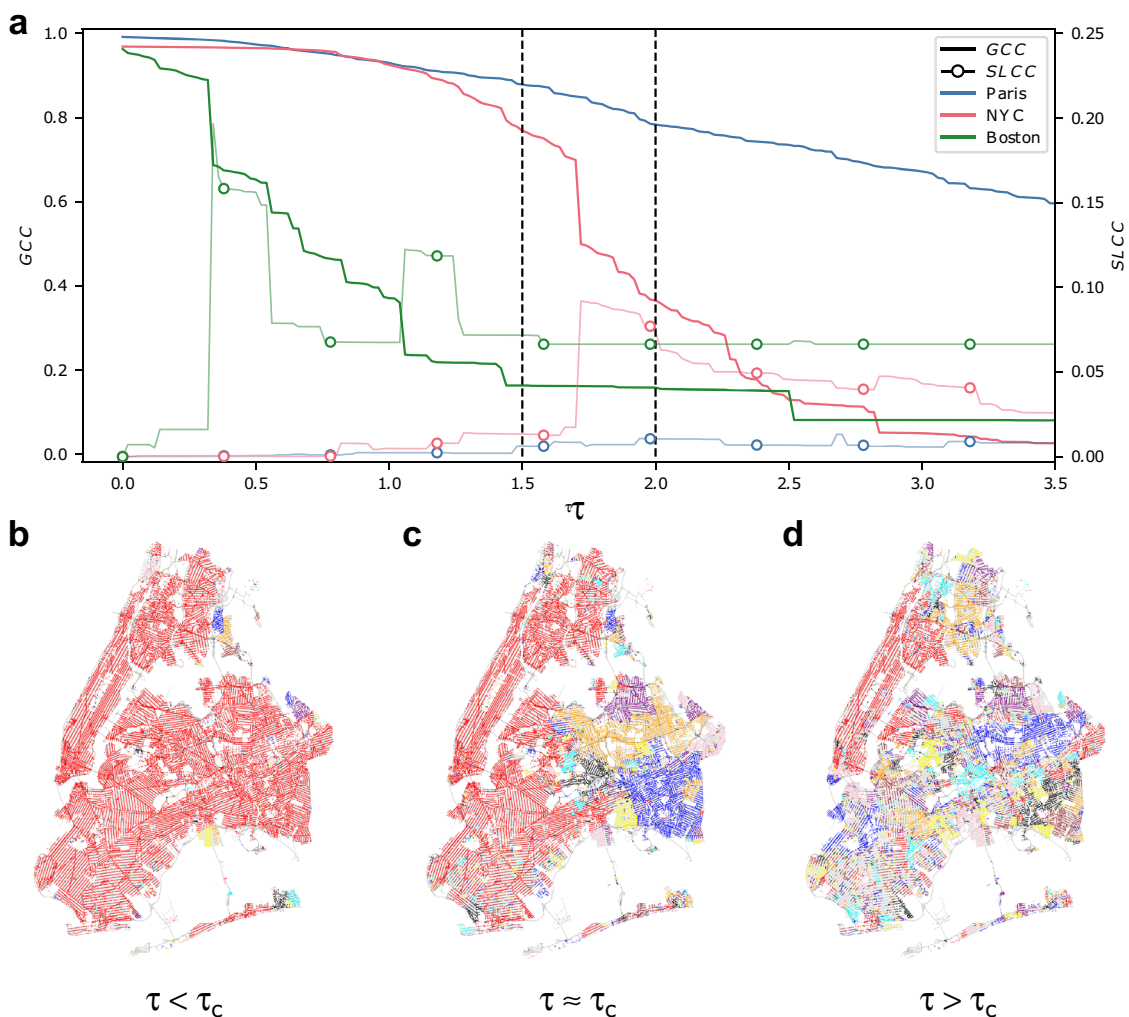


**Fig. 3 Effective width ( $w^{\text{eff}}$ ) percolation in Boston, New York, and Paris.** **a** Change in the size of the giant component GCC of the sidewalk network of Boston (green), New York City (red) and Paris (blue), as edges are iteratively removed at the threshold  $\tau$ , from lower to higher  $w^{\text{eff}}$ . The evolution of the second largest connected component SLCC is represented as well (right y-axis). The three cities react differently to sidewalk segment removal, with a collapsed sidewalk network in Boston and New York beyond  $\tau = 2$  m. As a visual aid, two dashed vertical lines at 1.5 and 2 m refer to the minimal width range necessary for an individual to maintain social distancing recommendations. **b-d** Sidewalk edges are colored according to the connected component they belong to. These panels correspond to three snapshots of New York’s breakdown around its critical percolation point  $\tau_c \approx 1.6$  m: from a pre-critical state ( $\tau < \tau_c$ ), to a dysfunctional stage at  $\tau \approx \tau_c$ , where several small clusters coexist (note that sidewalk nodes are colored according to the connected component to which they belong).

distancing recommendations<sup>6</sup>, considering a small buffer distance separating pedestrians from the roadbed and from the buildings running parallel to the sidewalk<sup>23</sup>, see Fig. 2c.

Correspondingly, we represent two dashed vertical lines at  $\tau = 1.5$  and  $\tau = 2$  m in (Fig. 3a). Following the decline of GCC, we see how the sidewalk networks in Boston (green), New York (red) and Paris (blue) break down, as we iteratively remove sidewalks segments of effective width below a threshold of  $\tau$  meters. Boston’s sidewalk network collapses before reaching  $\tau = 0.5$  m, as indicated by the peak of the second giant component<sup>33,34</sup> SLCC =  $C_2/N$  (circles in the plot). At a width of 1.5 m, it is already below 20%. New York, instead, reaches the critical percolation point soon after the first limiting width,  $\tau_c \approx 1.6$  m, and deteriorates rapidly thereafter. Beyond a threshold of  $\tau = 2.5$  m the network has totally collapsed. Paris, finally, shows a much slower rate of decline: its giant component still holds ~80% of the sidewalk network together at  $\tau = 2$ , and its critical point is not in sight even at  $\tau = 3.5$ . These three percolation profiles –and those for the other seven cities, see Supplementary Note 4 and

associated figures– present markedly diverse behaviors, and raise questions regarding the differences of the underlying structures. From a topological perspective, the three sidewalk networks in Fig. 3–and the rest of cities studied here– are similar, with an homogeneous degree distribution around a well-defined average degree  $\langle k \rangle$ , in line with other urban infrastructure network<sup>29,35</sup>. Consequently, a random percolation process renders a similar outcome for all of them: see Supplementary Note 5. The difference might be sought in the specificities of the interplay between the uneven distribution of the physical features of sidewalks<sup>36</sup> (particularly, their width) both across space and between various segments and the pedestrian demand on those segments. Deeper insights into such interplay are offered in Supplementary Notes 4 and 5.

The maps in (Fig. 3b-d) present three snapshots of the percolation process for New York, i.e., before (Fig. 3b), around (Fig. 3c) and after (Fig. 3d)  $\tau_c$ . Visible to the naked eye, the city exhibits a large giant connected component (red) in the initial stage, although some isolated areas emerge in the periphery. For

intermediate  $\tau$  values, much of the borough of Queens is already detached from the GCC. By  $\tau > 2$ , most of the city has been divided into small, localised clusters, and only the central borough of Manhattan, together with the southern Bronx, retain a functional walking infrastructure.

*Open Streets on interdependent networks.* Treating the problem of sidewalk physical distancing from a network perspective allows us to propose improvements to the status quo that take into account the system-wide effects of any local intervention. Pandemic-related or not, all of the street pacification<sup>37,38</sup> solutions that have been implemented in recent years by cities on an ad hoc basis, e.g., for selected streets in commercial arteries, involve redistributing limited street space from cars to pedestrians<sup>8,39</sup>. This creates a sensitive situation: the sidewalk and road networks of a city are coupled, and their interdependency shapes the conditions for their simultaneous operation<sup>40,41</sup>. Thus, while closing a street to traffic may improve the robustness of the sidewalk network, it necessarily comes at a cost for the road network. This interplay –any change in one network affects the other– demands a balanced approach: one that guarantees the sustainability of both structures. In this context, network analysis stands as a key tool to design strategies that may help determine how many (and which) streets can be pacified, while avoiding the collapse of the road network's functionality.

Towards this objective, we propose a greedy heuristic to designate Open Streets. We iterate over the segments  $e_{ij}$  of the sidewalk network in ascending order of  $w_{ij}^{\text{eff}}$ , setting  $\tau = w_{ij}^{\text{eff}}$  and selecting the corresponding road segment adjacent to  $e_{ij}$ . We then consider removing the sidewalk segment, or removing its neighboring road segment and converting the roadbed to a pedestrian area. To do so, we determine which structure suffers least, in terms of connectivity loss (giant component relative size), when the corresponding edge is removed. If the greatest loss is for the sidewalk (road) network, we remove the road (sidewalk) edge. Note that such drastic action –edge removal– does not necessarily translate into complete segment blockage if actually implemented: road edge removal could correspond to street pacification, which may often imply speed reduction or traffic lane(s) loss<sup>37,39</sup>. In the case of an equivalent loss for both interdependent structures, the road edge is preserved (the corresponding sidewalk edge is removed) with probability  $p \sim E_{ij}^r$ , where  $E_{ij}^r$  is the edge betweenness centrality<sup>42–44</sup> of the adjacent road segment  $(i, j)$ , which quantifies the amount of shortest paths that traverse each network edge and is related to road flow<sup>45,46</sup> and congestion<sup>43,47</sup>. Conversely, the road segment  $(i, j)$  is removed (sidewalk is preserved) with probability  $1 - p$ . Because of the stochastic element introduced by this tie-breaking mechanism, the process was run 40 times for each city. The *rationale* behind this tie-breaking criterium is to set a bias towards preserving high-betweenness road segments, which are fundamental to ease traffic flow and prevent congestion<sup>43,48,49</sup>. Admittedly, raw betweenness values might not be accurate for traffic flow predictions, and yet they allow for a rough estimation of road importance within the network, which suffices for our purpose. This conservative strategy towards central roads will, in turn, restrain (as we will see) an excessive increase in travel time, alongside the more general goal of sustaining connectivity.

Figure 4 describes the outcome of this process for Boston, Paris and New York (panels a, b and c). The dashed line reproduces the evolution of  $GCC_s$  if no intervention takes place (GCC in Fig. 3), as a baseline reference. The blue and red solid, bold lines represent, respectively, the average evolution of the sidewalk and road networks' giant component under our proposed heuristics,  $GCC_s^*$  and  $GCC_r^*$ , in which the effort to sustain both networks'

functionality is shared. Notably, the collapse of Boston's sidewalk network is delayed significantly: in the range  $1.5 < \tau < 2$  the GCC witnesses gains of more than 60%. This success is at an affordable cost for the road network, which in the same range has lost roughly 5% of its connectivity. Worth mentioning, the stochastic rule in the heuristic renders heterogeneous results (individual realizations of the heuristic are represented by thin lines around the bold averages). This degree of variability is not observed in the other two cases (Paris and New York), with over 95% of the sidewalk network still connected in both cities, at a thresholding width of 2 m, and a compact distribution of the individual realisations. Furthermore, the sustainability of the sidewalk network is compatible with very little-to-no harm to the integrity of the road network, whose giant component  $GCC_r^*$  still connects almost 100% of nodes in its structure, for both cities. Note that this strategy does not imply that any segment below 2 m of effective width has been pacified, but just enough that both structures could endure.

The process, despite positive results, has unavoidably damaged the road network to some extent. Besides a small loss in connectivity, the gray line in Fig. 4a, b and c monitors how much travel times have, on average, increased due to street pacification ( $\Delta\langle L \rangle$ ). Note that these travel times take into account the varying speed limits of different road segments (see Supplementary Note 3), and are not merely topological or distance-based. It turns out that, both in Paris and New York city, average travel times for vehicles have increased by no more than a factor of 1.2, if we set a limit at  $\tau = 2$  m; on the other hand, Boston's increase at  $\tau = 2$  is by a factor of 1.8. Disaggregated analysis of the increase in travel times is shown in the hex-binned panels (Fig. 4d, e and f), to the level of individual path duration distribution up to 20 min. Layered on top of the hex-bins, the plots show the median (dots), surrounded by the area ranging between the 10 and 90 percentiles (transparent blue). Clearly, we can observe that most travel times for New York and Paris suffer an increase factor of 1.5 or less, suggesting that the final travel time ( $L_{ij}^*$ ) comes at an acceptable cost. The situation is worse for Boston, where the median trend shows a doubling of travel times.

Supplementary Note 4 and associated figures reproduce the same results for the other seven cities studied here. The shared-effort strategy renders an extraordinary improvement for all cities, with a pedestrian GCC  $\approx 0.75$  or more at  $\tau = 2$  m, and a road network GCC mostly undamaged. Again, these improvements have only a moderate effect on travel times in general, with the exception of Montreal, which shows a trend similar to Boston's. These relatively homogeneous results are striking, considering the highly diverse baselines (no intervention) of the ten cities: some collapse early on, while others endure even at high  $\tau$  values.

The insets in (Fig. 4d, e and f), and the corresponding ones in Supplementary Figures 4–10, provide further analysis regarding the effects our heuristic may have on road congestion. Specifically, we analyze the impact on network edge betweenness, which is closely related to network congestion<sup>43,44</sup>. Overall, we observe a contained increase in the betweenness of roads. There are a limited number of edges that see a large increase or decrease in the betweenness. Clearly, some of the interventions proposed by the automated heuristic may require more fine-grained analysis to understand the microscopic impacts on the road networks of a given city. Still, in light of these results, we can conclude that road edge removal has mostly relied on mild-to-low centrality edges, as we expected, enabling large increases in sidewalk connectivity, but with limited harm to the backbone of the road structure, all while preserving to a large extent the original pattern of pressure on the road network.

The proposed heuristic is successful at both preventing an early collapse of sidewalk and road networks, and at maintaining

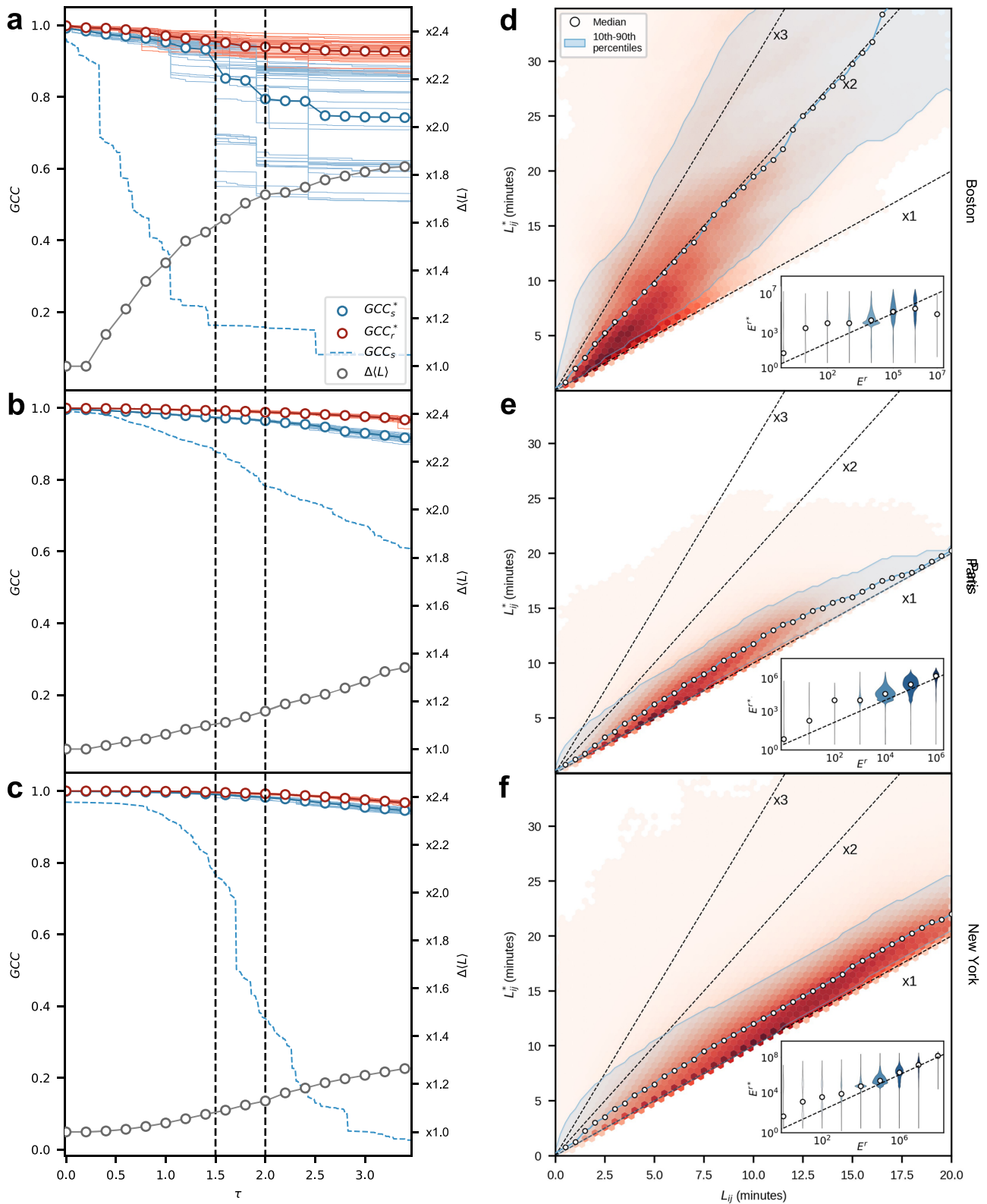


**Fig. 4 Results of the Open Streets shared-effort heuristic.** As can be seen in (a), (b), and (c), applying the process to Boston, New York City and Paris leads to significant gains for the sidewalk network with respect to the case of no intervention (blue dashed line). In addition, the road network begins to lose some connectivity as higher-width sidewalks are pedestrianised, but these losses are relatively small. The (d), (e) and (f) show the distribution of the increase in average path lengths (in minutes) for drivers when the process has been run up to sidewalks of 5 m in width. While removed streets from the road network clearly implies longer travel times for cars, these plots show quite forcefully that the costs are relatively low and concentrated around short-to-medium paths. Figure insets analyse the effects the heuristic has on the betweenness of roads,  $E^r$  corresponds to the initial betweenness value and  $E^{r*}$  to the road betweenness after the heuristic has been applied.

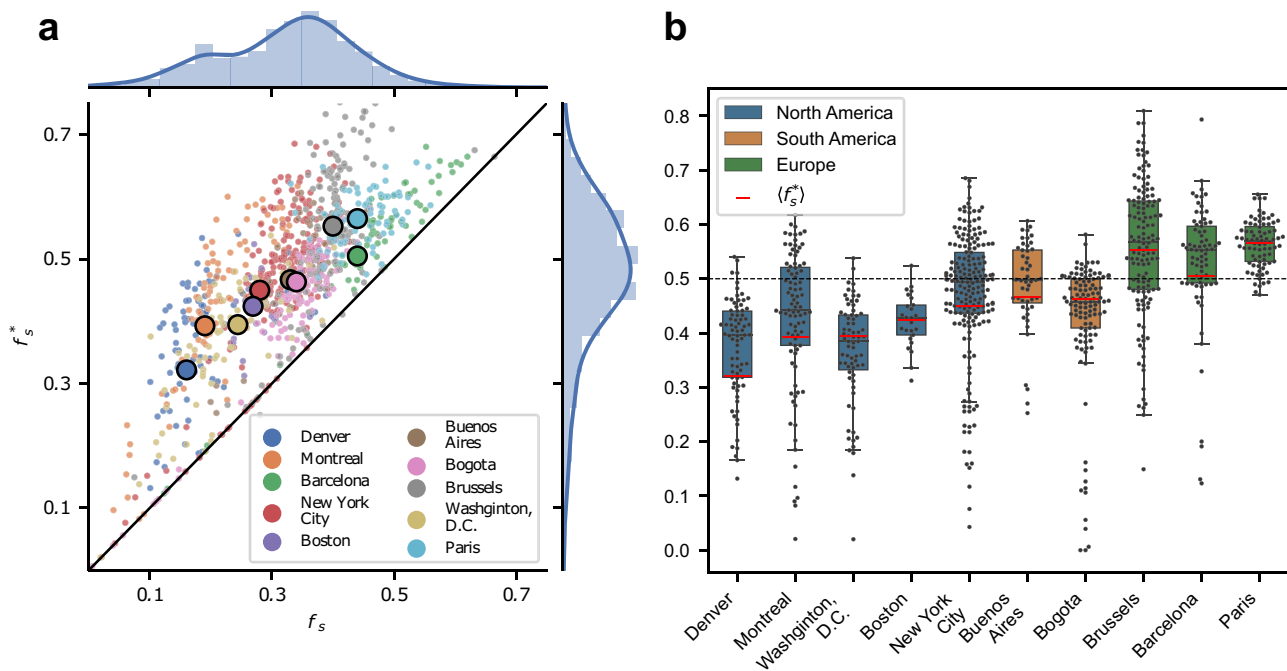


**Fig. 5** Distribution of public space, post-intervention at  $\tau = 2$ . **a** The scatterplot compares the amount of sidewalk share before and after the proposed intervention. Clearly, opening streets pedestrians to promote social distancing also has an effect on the overall distribution of space between pedestrians and cars, as illustrated here (the solid line with slope 1 is a guideline to the eye). **b** The box-plots (median in dark gray) display the distribution of space for all the cities for which the sidewalk geometries were gathered, now considering the gains in sidewalk share. To ease comparison, cities in the x-axis are sorted in the same order as in Fig. 1 in the same order. The average sidewalk share  $\langle f_s \rangle$  is marked in red.

vehicle travel times at a reasonable level. In addition, as a necessary side-effect, street pacification alters the street space share between sidewalks and roads<sup>39</sup> discussed in the beginning of this work. Figure 5 repeats the results shown in Fig. 1 for the 10 cities under study, except that the area corresponding to pacified roadbeds is now assigned to the existing sidewalk. The scatter plot in Fig. 5a plots the post-intervention sidewalk space share  $f_s^*$  against the original  $f_s$  for each district (smaller dots), as well as global city averages (larger dots). The marginal distributions pre- (top) and post-intervention (right) are also shown, evidencing a notable shift towards more balanced road-sidewalk space share. Figure 5b shows the new distribution of space share in each city, preserving the order as they were laid out in (Fig. 1). Clearly, the post-intervention scenario is more compact, with most cities –and districts within them– presenting a balanced  $0.4 < f_s^* < 0.6$ .

## Conclusion

The disruptions to daily life provoked by the COVID-19 pandemic have uncovered, or in some cases intensified, the need to rethink public space share, and to bolster active forms of mobility through concrete interventions. The idea of Open Streets—whether expressed through temporary or permanent sidewalk widenings, stringent speed limits or total traffic closures—is simple yet bold in a world of cities where automobiles still, by and large, dominate. Nevertheless, despite the significant public attention given to the issue, it is difficult if not impossible to find a large-scale, quantitative assessment of the way in which cities might handle the interlocking challenges that pedestrianisation and street pacification pose in pandemic and post-pandemic cities. Such a gap is not surprising: a lack of wide-spread data and standardized methods has prevented the development of a literature on the subject comparable to that of their counterpart road networks, making sidewalk networks perhaps the most neglected piece of our urban transportation infrastructure since long before the pandemic’s emergence. This work is, to the best of

our knowledge, the first to address, in a systematic and city-wide manner, the inadequacy of our cities’ sidewalk infrastructure for an equitable public space sharing, in the context of the ongoing pandemic and beyond.

This inadequacy is already apparent from the general evidence of the imbalanced distribution of public space. The informal impression that most street space is devoted to cars is accurately confirmed for a diverse selection of cities which, we suspect, are good representatives of the situation elsewhere –at least with regard to large urban areas. Notably, the inequalities between cities seem to indicate a range of possible functional distributions of urban street space, opening up possibilities for a reorganization of that space towards more socially optimal arrangements. Connecting these sidewalk geometries with two simple rules (change in direction or surface), we construct city-wide, richly-attributed sidewalk networks. These are represented as undirected, spatially-embedded, weighted structures, which can now be analysed within the framework of urban complex networks. A flow-sensitive, width-based targeted attack percolation process carried on the cities of study reveals that current sidewalk infrastructure becomes, if no intervention is in place, severely fragmented when stringent social distancing recommendations are taken into account, with many parts of the city mutually inaccessible on foot.

City governments have and exercise the power to facilitate physical distancing by pacifying streets, even at the cost of increasing inefficiencies for drivers. Without the underlying structure of the sidewalk network, however, it is not possible to assess the consequences of manually selected interventions at the neighborhood or city-wide levels. Road networks must be treated with care in order not to collapse vehicle mobility in cities. Street pacification thus demands that careful attention be given to the interdependencies between a city’s sidewalk and road networks, making a systemic, data-driven strategy necessary. To this end, we propose an heuristic that emphasizes the connectivity of both

the sidewalk and road networks, as well as the efficiency of the latter, with considerable gains for all the cities studied –despite the inherent limitations of working in a domain where empirical data are scarce. Also, an added benefit of the proposed strategy renders a more balanced distribution of street space for all cities under study.

We foresee that richly-attributed sidewalk networks will trigger much needed research on a wealth of topics that precede, and will no doubt extend beyond, the current health crisis. To start with, future efforts may try to overcome some of the idealisations in the present work, addressing, for example, the open discussion concerning which aspects of the built environment have an impact on pedestrian demand, including (but not limited to) block size, intersection density, diversity of services, and quality of infrastructure<sup>50</sup>, or the interplay between pedestrian routing and safety<sup>17</sup>, to name a few.

It appears clear that the pandemic has revealed an underlying tension concerning the design of our public space. By now, some major cities such as Paris and Barcelona have committed to maintaining and expanding the street pacification strategies implemented over the past year. As such strategies become another among many<sup>20,51</sup> long-term actions towards the end of car-dominated cities, empirically-grounded, systems-level planning tools like the one developed here will become increasingly relevant. Beyond this, the horizons for the study of sidewalks as networks are broad. Starting with the general lack of available public data on sidewalk infrastructure, these efforts can take several directions, from a theoretical understanding of the features of sidewalk networks, to practical issues like customized accessible sidewalk routing for those with and without mobility constraints<sup>52</sup>.

## Methods

**Data sources.** All data used was derived from publicly available open data sources.

**Open data on public space.** As mentioned in the main text, public data on sidewalk infrastructure is not standardised to the same extent as road network data. Many municipal open data portals lack generally available sidewalk data entirely. When available, sidewalk datasets generally take the form either of sets of sidewalk centerlines, or sets of sidewalk polygons. The latter is considerably more common, and also provides implicit information on the width of sidewalks. For this reason, the sidewalk data gathered for this work was restricted to cities with an available sidewalk polygon dataset. However, the algorithm for network construction could be easily adapted for other types of sidewalk data.

Supplementary Table 1 lists the public sources from which sidewalk geometries have been collected. Note that the formats in which these data are encoded varies from city to city.

**OpenStreetMap road networks.** Road network geometries were extracted from OpenStreetMap (OSM)<sup>53</sup> using the OSMnx Python package<sup>54</sup>, which provides a simple interface for querying OSM data. The package was used to extract the edges and nodes of the “Drive” and “Walk” networks of each city. The “Drive” network was used as a basis for sidewalk network construction, and later as the road network for the purposes of the Street Pedestrianization process (see final two sections below). The “Walk” network, which was filtered to only include those edges with a “highway” tag of “pedestrian”, “path”, or “living street”, was incorporated into the sidewalk network.

**Population data.** Empirical population data from open government sources serves as one of the three empirical inputs, along with point-of-interest (POI) data and empirical pedestrian count data (both described below), for the estimation of our pedestrian OD matrices for each city of study. As the cities are located in various countries, the population data came from differing sources, which are enumerated in Supplementary Table 2. However, all sources were made up of relatively small polygons (containing from 1 to a handful of city blocks, depending on the city), allowing for a good level of spatial resolution. The distribution of population density across all 10 cities is visualized, along with the POI data described below, in Supplementary Fig. 3.

**Point-of-interest data.** POI data was used along with the population data described above, and empirical pedestrian count data, to estimate our pedestrian OD matrices for each city of study. All POI data except for Denver’s was derived from

Foursquare<sup>55,56</sup>, a location-based social network. Foursquare POIs are hierarchically categorized into different uses (i.e., Restaurant → Chinese Restaurant), but these were not used. Instead, all POIs were considered homogeneously attractive to pedestrians. Potential duplicate POIs, those sharing the same category and location, were filtered from the dataset. Denver’s POIs were derived from OpenStreetMap<sup>53</sup>, which provides a similar format to Foursquare, in addition to also being crowd-sourced. More information on the spatial distribution of these points, which differed depending on the city, can be found in Supplementary Fig. 3.

**Street space distribution calculations.** For the purposes of this study, urban space was divided into 4 broad categories: Road, Sidewalk, Buildings, and Parkland. The focus of our analysis of public space was on the distribution of street space between cars and pedestrians. Accordingly, Buildings and Parkland were not considered in this work. For the purposes of calculating the area taken up by Road, datasets of roadbed polygons were used, when available. Otherwise, roadbed polygons were calculated as the area left over after subtracting all other categories of public space from the city (Buildings, Parkland, and Sidewalk).

**Sidewalk network construction.** Sidewalk networks were constructed using the two inputs of municipal sidewalk geometry data and road data from OpenStreetMap<sup>53</sup>. Each sidewalk geometry was assigned to a city block, and nodes were placed along the edge of the sidewalks at the points closest to that block’s corresponding road network intersection. Sidewalk geometries in line form were split at the location of these nodes to form network links. Finally, crossings were added to connect adjacent nodes from different blocks. More details on sidewalk network construction can be found in Supplementary Note 1.

**Pedestrian dynamics, sidewalk occupancy and effective width.** Access to real data on sidewalk use and demand is scarce and difficult to obtain. Open source alternatives (e.g., Twitter geotagged samples<sup>57</sup>) offer sparse datasets (in time and space) which make it nearly impossible to extract sidewalk occupancy with adequate precision. In addition, most of this data is quite noisy if one needs to precisely determine whether a data point is on the sidewalk.

Given these difficulties, and inspired by Yang et al.<sup>58</sup>, we obtain time-resolved sidewalk demand using a series of estimated Origin-Destination (OD) matrices, generated independently for each city of study. Each OD matrix is built upon three empirical inputs: geographic population data obtained from government Open Data portals (see Supplementary Table 3), point-of-interest (POI) data from Foursquare<sup>55,56</sup> (a location-based social network), and real pedestrian flow samples obtained through the company TC-Street (<https://www.tc-street.com/>). Each entry,  $o_{ij}$ , of the resulting OD matrix (of size  $N \times N$ , where  $N$  is the number of nodes in the city’s sidewalk network) represents the amount of people, per time step, who begin a journey departing from location  $i$  to destination  $j$ . Note that, as defined, the OD matrix has units pedestrians per time-step, and thus, can be used to estimate time-resolved sidewalk demand. As in<sup>45,46,48</sup>, the OD matrix will be fed to the calculation of the edge betweenness centrality of our distance weighted sidewalk networks. The effective edge betweenness will keep consistency with respect to the units of the OD matrix, thus it will provide us with the expected amount of pedestrians that get into each network edge per time step. Eventually, with some minimal additional considerations, this will result in the necessary time-resolved pedestrian occupancy of each sidewalk segment.

**OD matrix estimation.** Each OD matrix is constructed following the common gravitational analogy wherein those nodes of the sidewalk network containing the most services (i.e., having the most mass) are the most attractive to pedestrians<sup>58</sup>. To this end, we start by defining two vectors,  $p \in \mathbb{R}^N$  and  $s \in \mathbb{R}^N$  that correspond, respectively, to the population and the number of POIs present at each network node. Population data are aggregated in non-overlapping small polygons (e.g., census tracts in the US). Thus, every network node falls within exactly one population polygon. The assignment of population to a node  $i$ ,  $p_i$ , is simply an even distribution of the population in its polygon among the nodes of the sidewalk network that fall within it. Thus, if a polygon has a population of 100, and contains 4 nodes, each node will be assigned 25 pedestrians. On the other hand, the assignment of POIs to a node  $i$ ,  $s_i$ , is simply performed considering the closest Euclidean distance. This procedure can be efficiently performed using a Voronoi tessellation with cell centers corresponding to the network nodes: for each node  $i$ ,  $s_i$  will count the number of POIs that fall within  $i$ ’s Voronoi cell.

Subsequently, on the basis of vectors  $p$  and  $s$ , we estimate the different entries of the OD matrix. It is well-known that pedestrian mobility is strongly constrained by distance<sup>32</sup>. As such, we bias pedestrian destinations towards closer POIs. Specifically, we offset the attraction of the mass of POIs at a node  $i$ ,  $s_i$ , by a distance decay, following a half-normal distribution with a scale parameter  $\sigma$ . Applied to our problem, we fit  $\sigma$  such that 95% of trips fall within a Euclidean distance equivalent to the length a pedestrian will walk in 20 min at 5 km/h (1.4 m/s)<sup>59</sup>, giving  $\sigma = 855$  for a distance of ~1670 m. According to this scheme, the attraction of a destination  $j$  from a location  $i$  can be obtained as:

$$a_{ij} = \frac{s_j f(d_{ij}; \sigma)}{\sum_{k=1}^N s_k f(d_{ik}; \sigma)} \quad (1)$$

where  $f(d; \sigma)$  is the probability density function of the aforementioned half-normal distribution, and  $d$  indicates the Euclidean distance between  $i$  and  $j$ . Note that, Eq. (1) is normalized to ensure that  $\sum_j a_{ij} = 1$  for any  $i$ . Thus, each row  $a_i$  can be thought of as a vector describing the probability of a pedestrian choosing to visit POI at node  $j \neq i$  if she resides at node  $i$ . We finally obtain the entries  $o_{ij}$  of the OD matrix as:

$$o_{ij} = p_i a_{ij} u_j \tag{2}$$

where  $u_j \in [0, 1]$  represents the pedestrian demand for urban services at location  $j$  per time step. In the extreme,  $u_j = 1$  indicates that, at each time step, every citizen will start a trip to use a service at location  $j$ . Lower values indicate less frequency on the usage of services. The parameter  $u_j$  is obtained considering real sidewalk pedestrian counts, as shown later on.

**Pedestrian flows estimation.** So far,  $o_{ij}$  encodes the number of pedestrians departing from  $i$  and heading towards  $j$  per time step. The occupancy of each individual sidewalk segment will depend on the routes that those pedestrians will take, considering all intermediate edges. To find out these occupancies, we employ the edge betweenness, a well-known centrality measure for networks.

Edge betweenness accounts for the fraction of shortest paths that pass through each edge  $(i, j)$ , of a network. Although it is usually considered a structural descriptor, with a minimum change in our interpretation<sup>47,60</sup> it can also take a temporal dimension crucial to estimate traffic across a network's nodes and edges. To see how, let us consider a discrete process that generates elements (pedestrians, packets, etc.) at node  $k$  with a fixed destination  $\ell$ , at a rate  $o_{k\ell}$ . After their generation, and during the following time steps, these elements traverse the network, following a shortest path, towards their destination  $\ell$ . Once arrived, the elements are removed from the network. In this situation, each edge  $(i, j)$  traversed by the navigating element can keep record of the elements that traverse it per time step. Assuming a non-congested regime, a single shortest path between  $k$  and  $\ell$ , and assuming that all elements have the same velocity, elements should pass through the network edges at rate  $o_{k\ell}$ . If we now restrict the betweenness computation of edge  $(i, j)$  to only those paths that go from  $k$  to  $\ell$ ,  $E_{ij}^{(k\ell)}$ , the rate at which elements pass through the edge should be equivalent to:  $o_{k\ell} E_{ij}^{(k\ell)}$ . Note that  $E_{ij}^{(k\ell)}$  is 1 if all shortest paths between  $k$  and  $\ell$  traverse edge  $(i, j)$ ; otherwise  $E_{ij}^{(k\ell)}$  is the fraction of shortest paths between  $k$  and  $\ell$  traverse edge  $(i, j)$ , as in the original definition of betweenness centrality<sup>42</sup>.

Following a similar reasoning, we can account for all generation rates indicated by our OD matrix to estimate the input rate of any edge of the network. This brings us to a generalisation of the concept of betweenness to consider specific OD matrices<sup>45,46</sup>:

$$E_{ij} = \sum_{k \neq \ell} o_{k\ell} E_{ij}^{(k\ell)} = \sum_{k \neq \ell} o_{k\ell} \frac{\phi_{k\ell}(i, j)}{\phi_{k\ell}} \tag{3}$$

where  $\phi_{k\ell}$  corresponds to the number of shortest paths between  $k$  and  $\ell$ ,  $\phi_{k\ell}(i, j)$  to the number of shortest paths between  $k$  and  $\ell$  that traverse edge  $(i, j)$ , and  $o_{k\ell}$  to the generation rate of elements willing to navigate from  $k$  to  $\ell$  (that is, the entries of our OD matrix). This modified version of the edge betweenness centrality is computed with an efficient adaptation of the Brandes algorithm<sup>61</sup>.

**Fitting pedestrian demand.** We cannot continue the proposed pipeline unless we find a way to determine  $u_j$ , i.e., pedestrian demand for urban services at location  $j$  per time step. Only then can the OD matrix be conveniently scaled (Eq. (2)), and plugged into Eq. (3). First, since  $u_j$  is a rate, we need to define a suitable time-step. We settle on one minute as an appropriate length, allowing for fine-grained detail while not relying excessively on the quality of our input data. Then, we take daily pedestrian count data for a selected sidewalk segment in the center of Barcelona, provided by TC-Street. These coarse-grained data are adequately disaggregated at the scale of our time-step to obtain sidewalk demand per minute. For this down-sampling we, first, collected a realistic service usage distribution from Google Places, estimating hourly flows across that segment. Subsequently, flows within each hour were divided uniformly to obtain a flow-per-minute. The highest of those flows ( $\approx 11$  people per minute in the afternoon peak hour) was selected to represent a worst-case scenario.

This value represents the empirical betweenness at the selected sidewalk, and parameter  $u_j$  can now be fitted so that our observation (11 people per minute) matches the betweenness of the corresponding sidewalk segment as defined in Eq. (3). The value of  $u_j$  was found to be 0.0127, which corresponds to a scenario in which 1.27% of the city population begins their designated OD-trip each minute. Due to the lack of data elsewhere, we set  $u_j = u \forall j$ , so that each element of  $o_{ij}$  is scaled by the same amount. For the same reason,  $u = 0.0127$  is used as well on the other cities under study. We are aware that this represents an oversimplification regarding the demand landscape for urban services, but we believe it to be a useful approximation based on widely-available data sources, making the approach scalable.

**Sidewalk occupancy estimation.** Up to now, our modified version of the directed betweenness of a given sidewalk segment,  $E_{ij}$  and  $E_{ji}$ , indicates the average number of pedestrians that enter the sidewalk edge  $(i, j)$  from each end node per minute.

We now address how this translates to time-resolved sidewalk occupancy, and how it relates to social distancing. Assuming, as before, that pedestrians walk at 1.4 m/s, the time  $t_{ij}$  that a pedestrian takes to traverse the sidewalk segment  $(i, j)$  can be obtained. Since pedestrians are assumed to enter and leave sidewalk segments at the same rate, the expected number of pedestrians walking from  $i$  to  $j$  on a given sidewalk segment at any moment can be estimated as:

$$h_{ij} = t_{ij} E_{ij} \tag{4}$$

Equation (4) provides the occupancy of each sidewalk of the network, but it does not incorporate any internal pedestrian dynamics –density-related speed changes<sup>59</sup>, pedestrian groupings, gait-related heterogeneities. In this simplified setting, we assume the flow within sidewalks is organised in lines, see Fig. 3a. From this assumption, we devise a simple formula to calculate the number of lines that would be formed by incoming pedestrians from each end. Simply stated, if the length of the segment is not sufficient to guarantee a given distance between consecutive pedestrians entering from the same end, a new line is formed. The number of lines  $q_{ij}$  on a given sidewalk segment can be obtained as:

$$q_{ij} = \left\lceil \frac{h_{ij}}{h_{ij}^*} \right\rceil \tag{5}$$

where  $h_{ij}^* = l_{ij}/d$  is the maximum number of pedestrians that a single line on a segment of length  $l_{ij}$  can contain, while maintaining a distance  $d$  (taken here as 2 m) between consecutive pedestrians. Finally, if the total number of lines present on a segment ( $\hat{q}_{ij} = q_{ij} + q_{ji}$ ) is larger than 1, the effective width of the sidewalk (in meters) is obtained as:

$$w_{ij}^{\text{eff}} = \frac{w_{ij} - 1 - 0.5\hat{q}_{ij}}{\hat{q}_{ij} - 1} \tag{6}$$

where  $w_{ij}$  is the raw width of the sidewalk segment, and 1 m is subtracted from the raw width to account for a small buffer distance separating pedestrians from the roadbed (0.5 m) and from the buildings running parallel to the sidewalk (0.5 m). Also, each line is assumed to span 0.5 m, i.e., the shoulder breadth of an adult pedestrian. In the denominator,  $\hat{q}_{ij} - 1$  accounts for the number of empty spaces separating the adjacent lines of pedestrians (see Fig. 2b for a visual representation of this calculation). If  $\hat{q}_{ij} \leq 1$ , then  $w_{ij}^{\text{eff}} = \infty$ , i.e., the segment has such low pedestrian flow that  $(i, j)$  is never deleted in the percolation process. Finally, note that the effective width of a segment can be negative. This corresponds to the (sadly frequent) situation in which  $\hat{q}_{ij} > 1$  and  $w_{ij} \leq 2$ , and it explains why some cities have a  $GCC < 1$  already at the onset of the percolation process, when  $\tau = 0$  (see for instance Boston and New York in Fig. 3a, and several more in Supplementary Note 4). Supplementary Table 3 details reports on both the percentage of “frozen” ( $w_{ij}^{\text{eff}} = \infty$ ) and negative ( $w_{ij}^{\text{eff}} < 0$ ) links for each city.

**Effective width percolation.** As described in the text, for the purposes of percolation, the edges of the sidewalk network were sorted by effective width  $w^{\text{eff}}$  from lowest to highest, excluding pedestrian streets, crosswalks, and low-flow links (see above on sidewalk occupancy estimation), whose widths are set to infinity. Accordingly, the first edge to be percolated is the narrowest sidewalk in the network, and percolated edges become progressively wider from there. Networks were imported from geometric (ShapeFile) format into the Python implementation of the Igraph library<sup>62</sup>.

**Calculating the change in street space distribution after intervention.** As described in the text, pacifying traffic to convert a road segment into an Open Street necessarily increases the amount of street space dedicated to pedestrians<sup>39</sup>. Each road segment was assigned a portion of the total roadbed area which, when the segment is blocked, is considered as “sidewalk” for the purposes of calculating the distribution of street space. Similar to the method used to calculate sidewalk width, this area was taken as the part of the total roadbed area that was closer to the given road segment than to any other segment.

**Data availability**

The sidewalk networks used to produce the results of this work are available at OSF with the identifier <https://doi.org/10.17605/OSF.IO/94TDC>. The data on empirical segment-level pedestrian flows used to estimate the OD matrices are available from TC-Street, but were used under license for the current study, and are not publicly available. Data are however available from the authors upon reasonable request and with permission of TC-Street. All other data sources used are available from open data providers (see the data sources section of “Methods”, and Supplementary Notes 1, 2, and 3).

**Code availability**

The software code used to estimate the pedestrian OD matrices for each city, as well as the code to calculate the time-resolved edge betweenness of the sidewalk networks, is available at Github with identifier <https://doi.org/10.5281/zenodo.4849662> (alternatively, [https://github.com/COSIN3-UOC/sidewalk\\_networks](https://github.com/COSIN3-UOC/sidewalk_networks)).

Received: 8 July 2021; Accepted: 28 July 2021;  
Published online: 26 August 2021

## References

- Bulfone, T. C., Malekinejad, M., Rutherford, G. W. & Razani, N. Outdoor transmission of SARS-CoV-2 and other respiratory viruses: a systematic review. *J. Infect. Dis.* **223**, 550–561 (2021).
- Slovic, P. Perception of risk. *Science* **236**, 280–285 (1987).
- Van Bavel, J. J. et al. Using social and behavioural science to support COVID-19 pandemic response. *Nat. Human Behav.* **4**, 460–471 (2020).
- Honey-Rosés, J. et al. The impact of COVID-19 on public space: an early review of the emerging questions—design, perceptions and inequities. *Cities Health* 1–17, <https://doi.org/10.1080/23748834.2020.1780074> (2020).
- Chu, D. K. et al. Physical distancing, face masks, and eye protection to prevent person-to-person transmission of SARS-CoV-2 and COVID-19: a systematic review and meta-analysis. *The Lancet* **395**, 1973–1987 (2020).
- Moving around during the COVID-19 outbreak. Tech. Rep., World Health Organization (2020).
- Sadik-Khan, J. Streets for pandemic response and recovery. Accessed: 7-8-2020.
- Combs, T. S. & Pardo, C. F. Shifting streets COVID-19 mobility data: findings from a global dataset and a research agenda for transport planning and policy. *Transp. Res. Interdiscip. Perspect.* **9**, 100322 (2021).
- Gössling, S., Choi, A., Dekker, K. & Metzler, D. The social cost of automobility, cycling and walking in the European Union. *Ecological Econ.* **158**, 65–74 (2019).
- Brooks, J. H., Tingay, R. & Varney, J. Social distancing and COVID-19: an unprecedented active transport public health opportunity. *Br. J. Sports Med.* **55**, 411–412 (2021).
- Kadkhoda, K. Herd immunity to COVID-19: alluring and elusive. *Am. J. Clin. Pathol.* **155**, 471–472 (2021).
- Wang, H. & Noland, R. B. Bikeshare and subway ridership changes during the COVID-19 pandemic in New York city. *Transport Policy* **106**, 262–270 (2021).
- Basu, R. & Ferreira, J. Sustainable mobility in auto-dominated metro Boston: challenges and opportunities post-COVID-19. *Transp. Policy* **103**, 197–210 (2021).
- Orro, A., Novales, M., Monteagudo, Á., Pérez-López, J.-B. & Bugarín, M. R. Impact on city bus transit services of the COVID-19 lockdown and return to the new normal: the case of A Coruña (Spain). *Sustainability* **12**, 7206 (2020).
- King, A. Two more coronaviruses may infect people. *Science* **372**, 893–893 (2021).
- World Health Organization. COVID-19 virtual press conference transcript - 28 december 2020. <https://www.who.int/publications/m/item/covid-19-virtual-press-conference-transcript-28-december-2020>.
- Bustos, C. et al. Explainable, automated urban interventions to improve pedestrian and vehicle safety. *Transp. Res. Part C: Emerg. Technol.* **125**, 103018 (2021).
- Toole, J. L., Ulm, M., González, M. C. & Bauer, D. Inferring land use from mobile phone activity. In *Proceedings of the ACM SIGKDD international workshop on Urban Computing*, 1–8 (2012).
- Stockmaier, S. et al. Infectious diseases and social distancing in nature. *Science* **371**, eabc8881 (2021).
- Batty, M. The coronavirus crisis: What will the post-pandemic city look like? *Environ. Plan. B: Urban Anal. City Sci.* **47**, 547–552 (2020).
- Mækelæ, M. J. et al. Perceived efficacy of COVID-19 restrictions, reactions and their impact on mental health during the early phase of the outbreak in six countries. *Royal Soc. Open Sci.* **7**, 200644 (2020).
- Colville-Andersen, M. *Copenhagenez*, chap. The arrogance of space (Island Press, Washington, DC, 2018).
- NACTO. *Urban street design guide* (Island Press/Center for Resource Economics Washington, DC, 2013).
- Troko, J. et al. Is public transport a risk factor for acute respiratory infection? *BMC Infect. Dis.* **11**, 1–6 (2011).
- De Vos, J. The effect of COVID-19 and subsequent social distancing on travel behavior. *Transp. Res. Interdiscip. Perspect.* **5**, 100121 (2020).
- Li, M. et al. Percolation on complex networks: Theory and application. *Phys. Reports* **907**, 1–68 (2021).
- Li, D. et al. Percolation transition in dynamical traffic network with evolving critical bottlenecks. *Proc. Natl. Acad. Sci.* **112**, 669–672 (2015).
- Arcaute, E. et al. Cities and regions in Britain through hierarchical percolation. *Royal Soc. Open Sci.* **3**, 150691 (2016).
- Abbar, S., Zanouda, T. & Borge-Holthoefer, J. Structural robustness and service reachability in urban settings. *Data Min. Knowl. Discov.* **32**, 830–847 (2018).
- Serok, N., Levy, O., Havlin, S. & Blumenfeld-Lieberthal, E. Unveiling the interrelations between the urban streets network and its dynamic traffic flows: planning implication. *Environ. Plan. B: Urban Anal. City Sci.* **46**, 1362–1376 (2019).
- Barrington-Leigh, C. & Millard-Ball, A. A global assessment of street-network sprawl. *PLoS One* **14**, e0223078 (2019).
- Daniels, R. & Mulley, C. Explaining walking distance to public transport: the dominance of public transport supply. *J. Transp. Land Use* **6**, 5–20 (2013).
- Janson, S., Knuth, D. E., Łuczak, T. & Pittel, B. The birth of the giant component. *Random Struct. Algorithms* **4**, 233–358 (1993).
- Molloy, M. & Reed, B. The size of the giant component of a random graph with a given degree sequence. *Comb. Probability Comput.* **7**, 295–305 (1998).
- Barthélemy, M. Spatial networks. *Phys. Reports* **499**, 1–101 (2011).
- Artime, O. & De Domenico, M. Percolation on feature-enriched interconnected systems. *Nat. Commun.* **12**, 1–12 (2021).
- Brindle, B. Traffic calming in Australia: a definition and commentary. *Australian Road Research* **21**, 37–55 (1991).
- United Nations Conference on Housing and Sustainable Urban Development (UN-HABITAT III).
- Mueller, N. et al. Changing the urban design of cities for health: the superblock model. *Environ. Int.* **134**, 105132 (2020).
- Karndacharuk, A., Wilson, D. J. & Dunn, R. A review of the evolution of shared (street) space concepts in urban environments. *Transp. Rev.* **34**, 190–220 (2014).
- Radicchi, F. Percolation in real interdependent networks. *Nat. Phys.* **11**, 597–602 (2015).
- Freeman, L. C. A set of measures of centrality based on betweenness. *Sociometry*. **16**, 35–41 (1977).
- Guimerà, R., Díaz-Guilera, A., Vega-Redondo, F., Cabrales, A. & Arenas, A. Optimal network topologies for local search with congestion. *Phys. Rev. Lett.* **89**, 248701 (2002).
- Solé-Ribalta, A., Gómez, S. & Arenas, A. Congestion induced by the structure of multiplex networks. *Phys. Rev. Lett.* **116**, 108701 (2016).
- Altshuler, Y., Puzis, R., Elovici, Y., Bekhor, S. & Pentland, A. Augmented betweenness centrality for mobility prediction in transportation networks. In *International Workshop on Finding Patterns of Human Behaviors in Networks and Mobility Data, NEMO11* (2011).
- Henry, E., Bonnetain, L., Furno, A., El Faouzi, N.-E. & Zimeo, E. Spatio-temporal correlations of betweenness centrality and traffic metrics. In *2019 6th International Conference on Models and Technologies for Intelligent Transportation Systems (MT-ITS)*, 1–10 (IEEE, 2019).
- Solé-Ribalta, A., Gómez, S. & Arenas, A. A model to identify urban traffic congestion hotspots in complex networks. *Royal Soc. Open Sci.* **3**, 160098 (2016).
- Solé-Ribalta, A., Gómez, S. & Arenas, A. Decongestion of urban areas with hotspot pricing. *Netw. Spatial Econ.* **18**, 33–50 (2018).
- Solé-Ribalta, A., Arenas, A. & Gómez, S. Effect of shortest path multiplicity on congestion of multiplex networks. *New J. Phys.* **21**, 035003 (2019).
- Ewing, R. & Cervero, R. Travel and the built environment: a meta-analysis. *J. Am. Planning Assoc.* **76**, 265–294 (2010).
- Xu, Y., Olmos, L. E., Abbar, S. & González, M. C. Deconstructing laws of accessibility and facility distribution in cities. *Sci. Adv.* **6**, eabb4112 (2020).
- Bolten, N. et al. Urban sidewalks: visualization and routing for individuals with limited mobility. In *Proceedings of the 1st International ACM SIGSPATIAL Workshop on Smart Cities and Urban Analytics*, 122–125 (2015).
- OpenStreetMap contributors. Planet dump retrieved from <https://planet.osm.org>. <https://www.openstreetmap.org> (2017).
- Boeing, G. Osmnx: new methods for acquiring, constructing, analyzing, and visualizing complex street networks. *Comput. Environ. Urban Syst.* **65**, 126–139 (2017).
- Yang, D., Zhang, D. & Qu, B. Participatory cultural mapping based on collective behavior data in location-based social networks. *ACM Trans. Intell. Syst. Technol. (TIST)* **7**, 30 (2016).
- Yang, D., Zhang, D., Chen, L. & Qu, B. Nationtelescope: Monitoring and visualizing large-scale collective behavior in LBSNs. *J. Netw. Comput. Appl.* **55**, 170–180 (2015).
- Bassolas, A., Lenormand, M., Tugores, A., Gonçalves, B. & Ramasco, J. J. Touristic site attractiveness seen through Twitter. *EPJ Data Sci.* **5**, 1–9 (2016).
- Yang, Y., Herrera, C., Eagle, N. & González, M. C. Limits of predictability in commuting flows in the absence of data for calibration. *Sci. Rep.* **4**, 1–9 (2014).
- Bosina, E. & Weidmann, U. Estimating pedestrian speed using aggregated literature data. *Phys. A: Stat. Mech. Appl.* **468**, 1–29 (2017).
- Meloni, S., Arenas, A. & Moreno, Y. Traffic-driven epidemic spreading in finite-size scale-free networks. *Proc. Natl. Acad. Sci.* **106**, 16897–16902 (2009).
- Brandes, U. A faster algorithm for betweenness centrality. *J. Math. Sociol.* **25**, 163–177 (2001).
- Csardi, G. & Nepusz, T. The Igraph software package for complex network research. *InterJournalComplex Syst.*, 1695 (2006). <http://igraph.org>.

## Acknowledgements

D.R., A.S.-R. and J.B.-H. acknowledge financial support from the Dirección General de Tráfico (Spain), Project No. SPIP2017-02263. DR acknowledges as well the support of a doctoral grant from the Universitat Oberta de Catalunya (UOC). On M.C.G.'s side, this

work was supported by the Berkeley DeepDrive (BDD) and the University of California Institute of Transportation Studies (UC ITS) research grants. We thank TC-Street for supporting this research with data on segment-level pedestrian flows in Barcelona.

### Author contributions

D.R., A.S.-R., M.C.G. and J.B.-H. designed research. D.R. collected and curated the data. D.R., A.S.-R., M.C.G. and J.B.-H. authors performed research, analysed the results and wrote the paper. D.R., A.S.-R., M.C.G. and J.B.-H. authors approved the final version.

### Competing interests

The authors declare no competing interests.

### Additional information

**Supplementary information** The online version contains supplementary material available at <https://doi.org/10.1038/s42005-021-00688-z>.

**Correspondence** and requests for materials should be addressed to J.B.-H.

**Peer review information** *Communications Physics* thanks the anonymous reviewers for their contribution to the peer review of this work.

**Reprints and permission information** is available at <http://www.nature.com/reprints>

**Publisher's note** Springer Nature remains neutral with regard to jurisdictional claims in published maps and institutional affiliations.



**Open Access** This article is licensed under a Creative Commons Attribution 4.0 International License, which permits use, sharing, adaptation, distribution and reproduction in any medium or format, as long as you give appropriate credit to the original author(s) and the source, provide a link to the Creative Commons license, and indicate if changes were made. The images or other third party material in this article are included in the article's Creative Commons license, unless indicated otherwise in a credit line to the material. If material is not included in the article's Creative Commons license and your intended use is not permitted by statutory regulation or exceeds the permitted use, you will need to obtain permission directly from the copyright holder. To view a copy of this license, visit <http://creativecommons.org/licenses/by/4.0/>.

© The Author(s) 2021, corrected publication 2021